Title

Electron/Hole Mobilities of Periodic DNA and Nucleobase Structures from Large-Scale DFT Calculations

Journal

The Journal of Physical Chemistry B, 127(26)

ISSN

1520-6106

Authors

Kwon, Hyuna
Kumar, Anshuman
Del Ben, Mauro
et al.

Publication Date

2023-07-06

DOI

10.1021/acs.jpcb.2c09141

Peer reviewed

THE JOURNAL OF PHYSICAL CHEMISTRY B
A JOURNAL OF THE AMERICAN CHEMICAL SOCIETY

pubs.acs.org/JPCB

Article

Electron/Hole Mobilities of Periodic DNA and Nucleobase Structures from Large-Scale DFT Calculations

Published as part of The Journal of Physical Chemistry virtual special issue "Early-Career and Emerging Researchers in Physical Chemistry Volume 2".

Hyuna Kwon, Anshuman Kumar, Mauro Del Ben, and Bryan M. Wong*

Cite This: *J. Phys. Chem. B* 2023, 127, 5755−5763

Read Online

ACCESS | Metrics & More | Article Recommendations | Supporting Information

ABSTRACT: Electron/hole transfer mechanisms in DNA and polynucleotide structures continue to garner considerable interest as emerging charge-transport systems and molecular electronics. To shed mechanistic insight into these electronic properties, we carried out large-scale density functional theory (DFT) calculations (up to 650 atoms) to systematically analyze the structural and electron/hole transport properties of fully periodic single- and double-stranded DNA. We examined the performance of various exchange−correlation functionals (LDA, BLYP, B3LYP, and B3LYP-D) and found that single-stranded thymine (T) and cytosine (C) are predominantly hole conductors, whereas single-stranded adenine (A) and guanine (G) are better electron conductors. For double-stranded DNA structures, the periodic A-T and G-C electronic band structures undergo a significant renormalization, which causes hole transport to only occur on the A and G nucleobases. Our calculations (1) provide new benchmarks for periodic nucleobase structures using dispersion-corrected hybrid functionals with large basis sets and (2) highlight the importance of dispersion effects for obtaining accurate geometries and electron/hole mobilities in these extended systems.

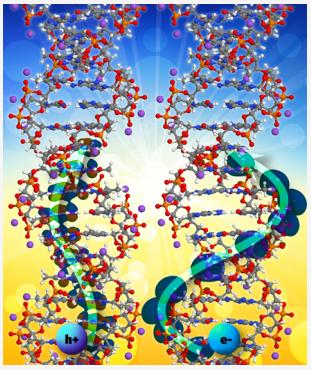

INTRODUCTION

Deoxyribonucleic acid (DNA) and polynucleotide structures continue to garner immense attention in various applications ranging from self-assembled biostructures to building blocks for next-generation electronics.[1−8] In recent years, DNA has attracted significant attention in nanoelectronics and information storage since it can adopt complex geometries and is inherently stable in a multitude of chemical environments.[9−15] Because of its one-dimensional (1D) structure of π-stacked nucleobases, early experimental efforts were intensely focused on the possibility of using DNA as a nanoscale conductor for enhanced electrical conductivity and charge transport.[16−20] However, subsequent experiments provided contradictory results, including suggestions that DNA is a conducting wire,[21] superconductor,[22] semiconductor,[23] or a wide-band gap insulator.[24,25] The discrepancies in these experimental results were attributed to variations in the DNA structures, such as the specific base sequence and the specific chemical environment used in the experiments.

On the theoretical side, numerous computational studies, including tight-binding models,[26,27] quantum chemistry calculations,[28−30] and quantum mechanics/molecular mechanics (QM/MM) studies[31−33] have been carried out on DNA and polynucleotide structures to predict their charge-transport properties. However, the vast majority of these computational studies focused on nucleobase oligomers and did not address band structure properties in a fully periodic geometry. While these oligomer calculations can provide a reasonable prediction of DNA properties, they are typically more appropriate for small molecular-like sections of DNA and cannot capture the full electronic transport behavior as a function of electron momentum. There have been a handful of theoretical studies on fully periodic DNA structures;[34−36] however, these prior studies either employed semilocal exchange−correlation functionals (known to underestimate band gaps) with minimal basis sets[33] or used Hartree−Fock calculations (which overestimate band gaps) on idealized geometries extracted from molecular dynamics simulations.[37,38]

To shed additional insight into the electronic properties of DNA and polynucleotide structures, we present large-scale density functional theory (DFT) calculations to systematically analyze their structural and electron/hole transport properties. We also examine the performance of various exchange−correlation functionals, ranging from local (LDA) to semilocal (BLYP), hybrid (B3LYP), and dispersion-corrected hybrid (B3LYP-D) methods on the electronic properties of single- and double-stranded DNA structures. However, it is important to

Received: December 31, 2022
Revised: June 2, 2023
Published: June 22, 2023

https://doi.org/10.1021/acs.jpcb.2c09141
J. Phys. Chem. B 2023, 127, 5755−5763

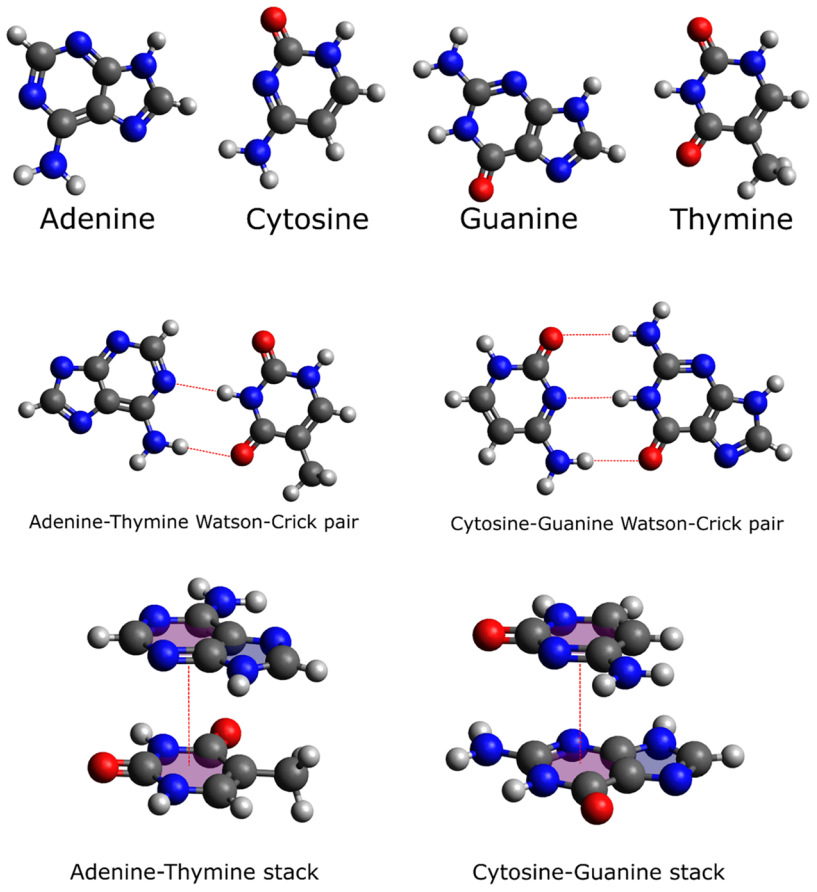

Figure 1. Molecular structures of DNA nucleobase monomers, stacked pairs, and Watson−Crick base pairs from the S22 dataset used as benchmarks in this work. The carbon, hydrogen, nitrogen, and oxygen atoms are depicted as gray, white, blue, and red spheres, respectively.

mention that the goal of our current study is not to resolve open issues on charge-transport mechanisms in DNA. Rather, the large-scale calculations presented in this work can serve as new reference benchmarks that are expected to be more accurate than the semilocal or Hartree−Fock calculations discussed previously.[39] Most notably, the B3LYP-D calculations in this work represent one of the first studies of periodic DNA and nucleobase structures using dispersion-corrected hybrid functionals for both full geometry optimizations and electronic band structures. Using these optimized geometries and band structures, we present electron/hole mobilities for various single- and double-strand DNA structures. Finally, our paper concludes with an analysis of orbitals and charge-transfer mechanisms to rationalize the electronic properties and electron/hole transport mechanisms in these complex nucleobase structures.

THEORY AND METHODOLOGY

All of the DFT calculations in this study were carried out with a massively parallelized version of the CRYSTAL14 program,[40] which can calculate nonlocal Hartree−Fock exchange with all-electron Gaussian basis sets and periodic boundary conditions. While our work focuses on ground-state electronic properties of periodic DNA, previous research by us has shown that the choice of exchange−correlation functional can also strongly affect the accuracy of excitation energies in DNA and RNA nucleobases.[41,42] As such, we evaluated a variety of exchange−correlation functionals to understand their effects on DNA electron/hole mobilities, including (1) LDA (local density approximation),[43] a semilocal functional derived from the exchange−correlation energy of a homogeneous electron gas, (2) BLYP (Becke exchange with Lee Yang Parr correlation),[44] a generalized gradient approximation functional without nonlocal exchange, (3) B3LYP,[45] a popular 3-parameter hybrid functional that contains a 20% fraction of Hartree−Fock exchange, and (4) B3LYP-D,[46] a dispersion-corrected version of the B3LYP hybrid functional.

Geometries for all single- and double-stranded DNA structures were optimized using a 6−31G(d,p) all-electron basis set with one-dimensional (1D) periodic boundary conditions along the helical axis. Since each of the phosphate groups along the backbone has a −1 charge, a single Na^+ cation was added near these groups to ensure charge neutrality of the entire periodic system. All of the structures examined in this work exhibit a full helical turn (i.e., 360°) with 10 nucleotides in a one-dimensional periodic unit cell. At these optimized geometries, single-point calculations were performed with a larger 6−311G(d,p) basis set with 100 *k*-points along the one-dimensional Brillouin zone to obtain the resulting electronic band structures. It is worth noting that the calculations on some of the periodic DNA strands were extremely computationally intensive due to the large size of these systems. For example, the largest of these structures (poly(A-T)) consists of 650 atoms and 9440 basis functions and, as such, constitutes one of the most extensive quantum mechanical studies of these periodic biological structures to date.

We briefly outline the deformation potential (DP) formalism[47,48] for calculating electron and hole mobilities (μ_e and μ_h,

https://doi.org/10.1021/acs.jpcb.2c09141
J. Phys. Chem. B 2023, 127, 5755−5763

respectively) for each of our DNA structures. Within this formalism, the electron or hole mobilities in a one-dimensional (1D) periodic system are given by

$$\mu_{e,h} = \frac{e\hbar^2 C}{(2\pi k_B T)^{1/2} |m^*_{e,h}|^{3/2} E_1^2} \quad (1)$$

where e is the charge of an electron, k_B is Boltzmann's constant, $\hbar$ is the reduced Planck constant, T is the temperature (set to 298 K in this study), and E_1 is the DP constant along the one-dimensional periodic direction. The latter is obtained by calculating the rate of change of the valence/conduction band edge with respect to strain. The elastic modulus of the system is given by $C = 1/a_0 \cdot \partial^2 E/\partial \varepsilon^2$, where E is the total energy of the system and ε is strain. The effective mass of the electrons and holes (m^*_e and m^*_h, respectively) was calculated at the conduction band minimum and valence band maximum, respectively, using the expression

$$\frac{1}{m^*_{e,h}} = \pm \frac{1}{\hbar^2} \frac{d^2 \epsilon_{c,v}}{dk^2} \quad (2)$$

The positive sign is taken for the (electron) conduction band (ϵ_c), and the negative sign corresponds to the (hole) valence band (ϵ_v). A total of 100 uniformly spaced points from Γ to the X point were used to calculate $m^*_{e,h}$.

Finally, the elastic constant C was calculated from a contraction−dilation displacement of the entire nucleotide strand using the following expression

$$C = l_o \frac{\partial^2 E}{\partial l^2}\bigg|_{l=l_o} \quad (3)$$

where l is the length of the DNA strand under tension/compression, E is the total energy per unit cell, and l_o is the equilibrium length. The periodic DNA strand was stretched/compressed at 0.5, 1.0, and 1.5% intervals with single-point energies calculated at each step. These seven data points ($\Delta l/l_o$ = 0, ±0.005, ±0.01, ±0.015) were then used to generate dilation-energy curves to obtain the elastic constant.

RESULTS AND DISCUSSION

Benchmark Calculations on Nucleotide Base Pairs. Before calculating electron/hole mobilities of the various DNA strands, we first assessed the accuracy of the LDA, BLYP, B3LYP, and B3LYP-D functionals for predicting nucleotide interaction energies when compared to the S22 benchmark dataset.[49] In particular, the S22 set contains several DNA nucleobase monomers (adenine, cytosine, guanine, and thymine), stacked pair geometries (adenine−thymine and guanine−cytosine), and a canonical Watson−Crick base pair (adenine−thymine and guanine−cytosine) calculated at a complete-basis-set-extrapolated CCSD(T) level of theory. Figure 1 depicts the molecular structures of the various base pair systems considered in this work, and Figure 2 compares the interaction energies obtained by the various functionals against the CCSD(T) benchmark values from the S22 dataset (numerical values and root-mean-square errors (RMSEs) are reported in Table 1).

As can be seen in Figure 2 and Table 1, the B3LYP-D and LDA functionals are in good and reasonable agreement, respectively, with the benchmark values; however, the BLYP and B3LYP methods yield more repulsive energies (i.e., more positive values) with errors larger than 2.0 kcal/mol. BLYP, a GGA functional, significantly reduces the over-binding tendency of LDA, which is exacerbated in monomer pairs (as opposed to stacks) since hydrogen bonding is prevalent in pairs but absent in stacks. The B3LYP and BLYP functionals underestimate binding energies compared to B3LYP-D since they do not include attractive dispersion interactions. While hybrid functionals such as B3LYP have long-range (nonlocal) effects through Hartree−Fock exchange, they remain local in correlation and, therefore, are unable to describe the R^{-6} asymptotic distance-dependence of dispersion forces correctly.[50] It is worth noting that while dispersion corrections give more accurate geometries, they do not address known limitations of B3LYP for long-range charge transfer/transport, particularly in molecular systems.[51−53] For the same reason, even though the B3LYP-D interaction energies give the best agreement with the CCSD(T) benchmarks in this study, the electronic couplings involved in the rates of charge transfer/transport in these systems can still incur large errors. Nevertheless, we have chosen to use B3LYP-D for our studies since (1) long-range-corrected functionals with 100% asymptotic exchange are not appropriate for neutrally charged periodic structures (since they neglect electron screening effects), and (2) the B3LYP-D functional has been shown to mimic screening effects (due to a fortuitous cancellation of errors) to give reasonable band gaps for periodic structures.[54−56]

The B3LYP functional gives weaker binding energies than the CCSD(T) benchmarks, and prior work by Zhang et al. suggested that this under-binding becomes more pronounced

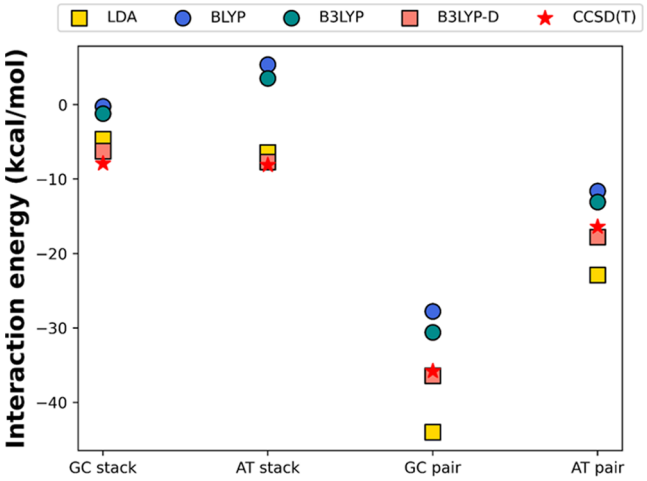

Figure 2. Interaction energies (in kcal/mol) of stacked and Watson−Crick pair configurations of GC and AT calculated at different levels of theory and compared to CCSD(T) benchmark values (denoted as red stars) from the S22 dataset.

Table 1. Comparison of Interaction Energies Predicted by LDA, BLYP, B3LYP, and B3LYP-D against CCSD(T) Reference Values from the S22 Dataset

	interaction energy (kcal/mol)				
	LDA	BLYP	B3LYP	B3LYP-D	CCSD(T)
AT stack	−6.42	5.39	3.53	−7.71	−8.10
AT pair	−22.90	−11.61	−13.09	−17.77	−16.40
GC stack	−4.65	−0.23	−1.20	−6.24	−7.90
GC pair	−44.00	−27.77	−30.60	−36.41	−35.80
RMSE	5.54	9.06	7.38	1.14	

https://doi.org/10.1021/acs.jpcb.2c09141
J. Phys. Chem. B 2023, 127, 5755−5763

with increasing molecular size.[57] As such, B3LYP will incur significant errors for the large periodic strands, as we demonstrate in the next section. Based on these benchmark calculations, the B3LYP-D functional most closely matches the CCSD(T) results, particularly for the van-der-Waals-stacked monomers.

Optimized Geometries of Single- and Double-Stranded DNA. With the individual nucleotide benchmarks calculated, we next optimized the geometries of various ssDNA and dsDNA systems: periodic adenine (poly(A)), thymine (poly(T)), cytosine (poly(C)), guanine (poly(G)), adenine−thymine (poly(A-T)), and guanine−cytosine (poly(G-C)). Figure 3 depicts magnified views of the optimized geometries

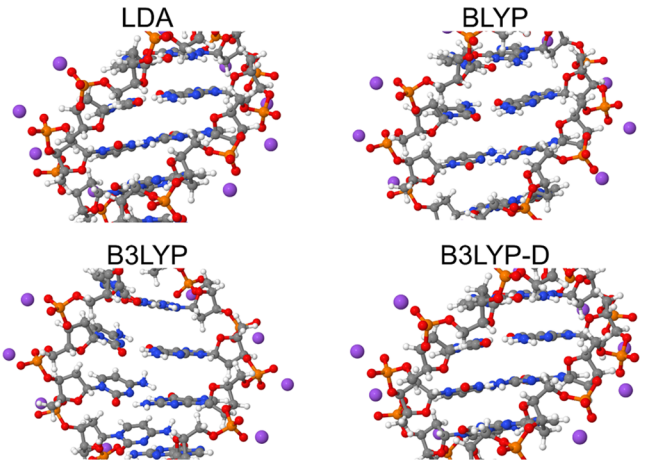

Figure 3. Geometries of periodic poly(G-C) obtained with the LDA, BLYP, B3LYP, and B3LYP-D functionals. Only LDA and B3LYP-D give stable structures, whereas the other functionals give unstable and distorted geometries between adjacent Watson−Crick pairs.

for the periodic poly(G-C) strands obtained with the LDA, BLYP, B3LYP, and B3LYP-D functionals. As seen in this figure, only LDA and B3LYP-D give structurally stable geometries (Cartesian coordinates for all of the B3LYP-D-optimized ssDNA and dsDNA structures can be found in the Supporting Information). In contrast, both the BLYP and B3LYP functionals produce geometries that are highly distorted in which the individual Watson−Crick base pairs are not even aligned in the same plane. A frequency analysis can give further information on structural stability; however, geometry optimizations of these large, periodic systems were already computationally expensive (requiring hundreds of thousands of CPU hours), and frequency calculations were out of reach for these structures. For this reason, we only present the structures in Figure 3, which clearly depict the base pairs to be misaligned with each other to depict the distortions/instabilities in these structures.

The structural deformations in these periodic strands are fully consistent with the benchmark calculations described in the previous section. In particular, our benchmark calculations on individual nucleotides showed that only LDA and B3LYP-D predict stable A-T and C-G stacks/Watson−Crick pairs in comparison to the CCSD(T) benchmarks. In contrast, both BLYP and B3LYP considerably underestimate these interaction energies. As a result, the under-binding tendencies in BLYP and B3LYP become even more pronounced in the periodic systems (since both stacking and Watson−Crick pairs are now present in the periodic system), leading to the geometric distortions seen in Figure 3. While Figure 3 only depicts the poly(G-C) strands for brevity, we observed similar geometric trends in poly(A-T) in which only LDA and B3LYP-D gave stable structures. Our results also corroborate previous molecular dynamics simulations on a DNA dodecamer, which suggested that the double-helical structure is not stable when dispersion interactions are not incorporated.[58]

Electron/Hole Mobilities. With the geometries of all of the periodic strands optimized, we now analyze electron/hole mobilities for the various ssDNA and dsDNA systems. For clarity, we only discuss electron/hole mobilities calculated at the B3LYP-D level of theory since this functional simultaneously gives stable geometries and reasonable band gaps[54−56] (LDA also gave stable geometries in our study but is well known for underestimating band gaps). It is worth noting that the choice of functionals, such as B3LYP-D, can influence the amount of negative charge attributed to the nucleobases. However, since wavefunction-based methods are currently prohibitive for obtaining more accurate charge analyses in these large periodic structures, we chose B3LYP-D as the best functional examined in our study for further analysis of our periodic DNA systems. Table 2 presents the lattice parameters, band gaps, and electron/hole masses (required for calculating electron/hole mobilities from eq 1), and Table 3 summarizes the electronic charge per nucleobase and the electron/hole mobilities of all ssDNA and dsDNA structures (electron/hole mobilities for other functionals are given in the Supporting Information).

Table 2. Lattice Parameters, Band Gaps, and Effective Masses of Holes/Electrons of Various Single- and Double-Strand DNA Systems Computed at the B3LYP-D/6−311g(d,p) Level of Theory

system	lattice parameter (Å)	band gap (eV)	m_e^* (m_0)	m_h^* (m_0)
poly(A)	32.22	3.92	7.39	10.13
poly(T)	29.70	3.12	32.02	2.00
poly(G)	31.39	3.66	10.12	50.36
poly(C)	30.74	3.22	17.86	3.25
poly(A-T)	31.29	3.23	8.86	17.74
poly(G-C)	32.45	1.39	22.74	2.69

Table 3. Electronic Charge Per Nucleobase and Electron/Hole Mobilities of Various Single- and Double-Strand DNA Systems Computed at the B3LYP-D/6−311g(d,p) Level of Theory

system	electronic charge per nucleobase (e)	electron mobility ($cm^2/V{\cdot}s$)	hole mobility ($cm^2/V{\cdot}s$)
poly(A)	−0.26 (A)	18.22	9.72
poly(T)	−0.20 (T)	4.08	22.33
poly(G)	−0.24 (G)	15.77	0.54
poly(C)	−0.18 (C)	4.09	39.81
poly(A-T)	−0.23 (A), −0.24 (T)	40.23	5.14
poly(G-C)	−0.21 (G), −0.17 (C)	9.59	19.38

Figure 4 shows that the highest occupied crystal orbitals (HOCOs) are localized on the nucleobase (regardless of nucleobase species) in all of the B3LYP-D-optimized ssDNA structures. In contrast, the lowest unoccupied crystal orbitals (LUCOs) are primarily found on the Na^+ cations and the phosphate backbone. Both of these HOCO and LUCO localization patterns are consistent with previous work,[35,36] which used Hartree−Fock calculations and small basis sets. Moreover, since the spatial distribution of the HOCO influences

https://doi.org/10.1021/acs.jpcb.2c09141
J. Phys. Chem. B 2023, 127, 5755−5763

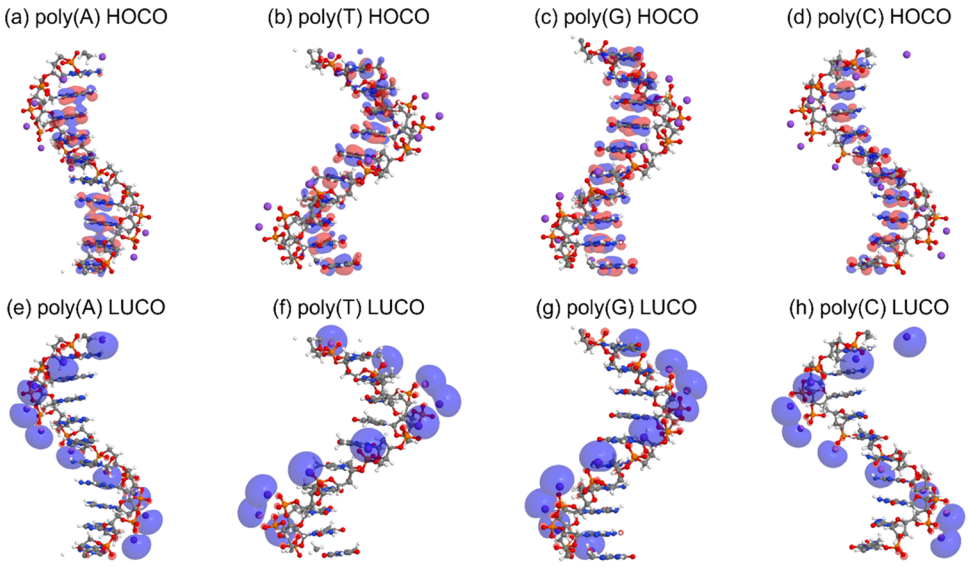

Figure 4. HOCOs and LUCOs of ssDNA obtained with the B3LYP-D functional.

the hole mobility, our calculations predict that hole transport in ssDNA occurs intramolecularly across the nucleobase stacks, whereas electron transport (which is determined by the LUCO) occurs across the Na^+ cations and phosphate backbone.

It is worth noting that the ssDNA structures with purine nucleobases (i.e., A and G) have a significantly lower hole mobility than the corresponding structures with pyrimidine nucleobases (i.e., T and C). This is due to the HOCOs in poly(A) and poly(G) being formed from the highest occupied molecular orbitals (HOMOs) of A and G (cf. Figure 5), which

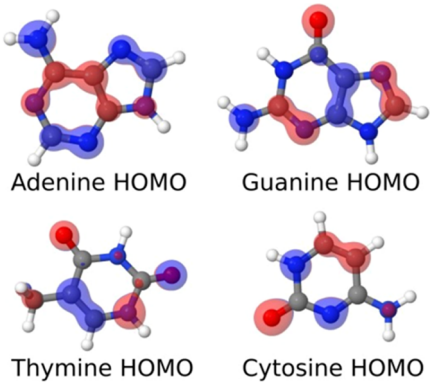

Figure 5. HOMOs of A, T, G, and C calculated at the B3LYP-D/6−311g(d,p) level of theory.

have an *antibonding* interaction in the helical ssDNA stacked geometry.[34] Conversely, the ssDNA structures with purine nucleobases have a significantly higher electron mobility than the corresponding structures with pyrimidine nucleobases. This trend arises from the LUCOs in poly(A) and poly(G) having a larger overlap than the corresponding LUCOs in poly(T) and poly(C), as can be seen in Figure 4. Furthermore, both A and G contain more sp^2 hybridized segments with highly electronegative atomic species (i.e., nitrogen and oxygen) than C and T. For example, A contains three sp^2 C═N units, and G has two C═N and one C═O unit; in contrast, C includes one C═O, one C═N, and one C═C unit, and T contains one C═C and two C═O units. This results in a partial negative charge on the nitrogen and oxygen atoms and a partial positive charge on the neighboring carbon atoms. In turn, this polarity of the sp^2 hybridized atoms can facilitate noncovalent interactions between nucleobases, leading to a larger electron mobility due to its increased electron affinity. As such, these chemical insights corroborate our results showing that purine nucleobases possess higher electron mobility than pyrimidine nucleobases.

It is also interesting to note that the electronic charge per nucleobase (cf. Table 3) is also correlated with the electron/hole mobility in the ssDNA structures. While our DFT calculations indicate that the nucleobases in all four of the ssDNA structures are negatively charged, nucleobases with the most negative charge (A and G) exhibit the highest electron mobilities, whereas nucleobases with the least negative charge (T and C) have the highest hole mobilities. Taken together, the HOCO/LUCO interactions and electronic charges in these ssDNA structures result in poly(T) and poly(C) being hole conductors, whereas poly(A) and poly(G) structures are better electron conductors.

Turning our attention to the dsDNA structures, Figure 6 shows that the HOCOs on these systems are localized on the A and G nucleobases in the poly(A-T) and poly(G-C) structures, respectively. As such, our calculations predict that hole transport in dsDNA occurs only across the purine (and not the pyrimidine) nucleobases in both these structures. In contrast, the LUCOs are localized on the Na^+ cations and the phosphate groups (proximal to the pyrimidine bases, C and T), indicating that electron transport occurs along the backbone in both structures. To visualize the HOCOs and LUCOs more easily, the Supporting Information provides three-dimensional (3D) animations of these orbitals for the poly(A-T) structure.

To understand the electronic interactions in these dsDNA structures more closely, Table 4 provides HOCO/LUCO energies of poly(A), poly(T), poly(A-T), poly(G), poly(C), and poly(G-C) calculated at the B3LYP-D/6−311g(d,p) level of theory, and Figure 7 plots their corresponding electronic band structures. It is worth noting that the electronic properties of poly(A-T) and poly(G-C) are more complex than their constituents and are not merely superpositions of the individual ssDNA poly(A) + poly(T) or poly(G) + poly(C) band structures. In particular, the right-most column of Figure 7

https://doi.org/10.1021/acs.jpcb.2c09141
J. Phys. Chem. B 2023, 127, 5755−5763

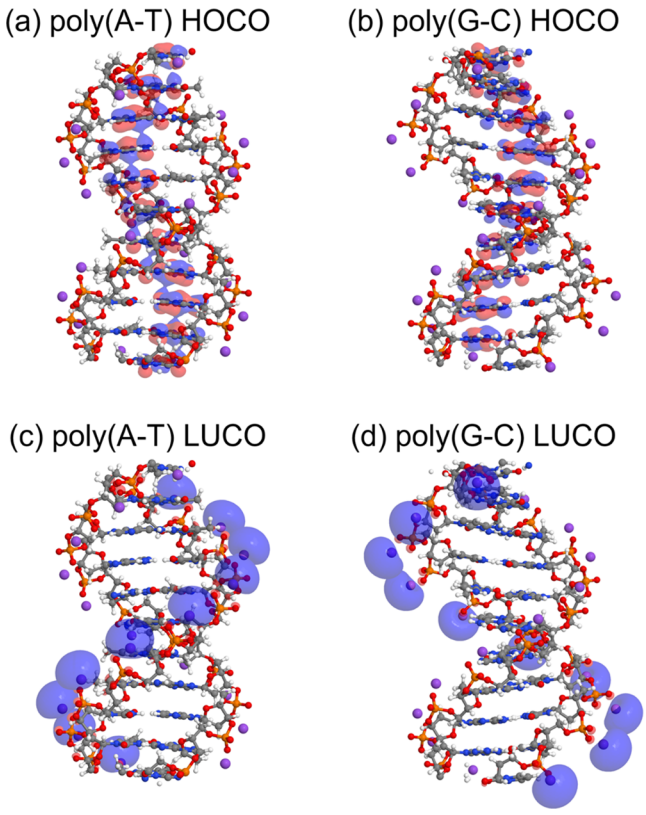

Figure 6. HOCOs and LUCOs of poly(A-T) and poly(G-C) calculated at the B3LYP-D/6−311g(d,p) level of theory.

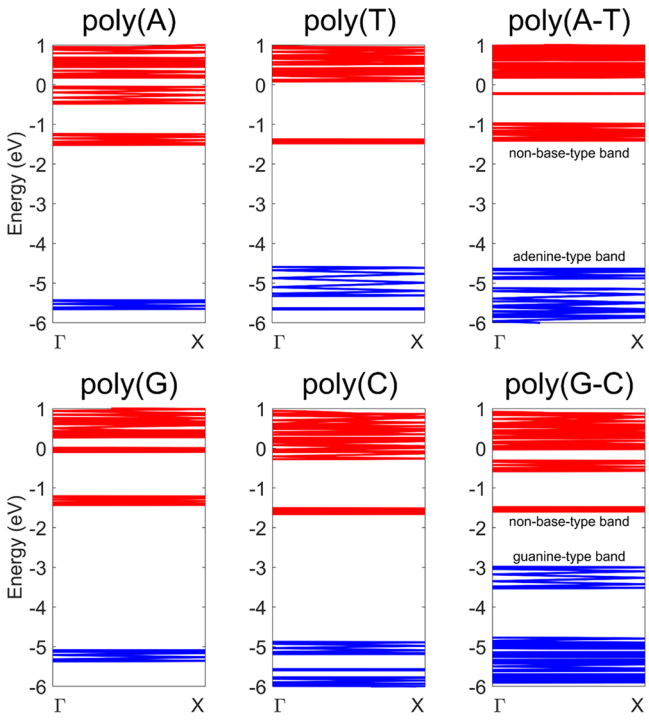

Figure 7. Band structures of poly(A), poly(T), poly(A-T), poly(G), poly(C), and poly(G-C) calculated at the B3LYP-D/6−311g(d,p) level of theory. The A- and G-type bands are pushed upward in the double-stranded poly(A-T) and poly(G-C) cases, respectively.

Table 4. HOCO and LUCO Energies of Various Single- and Double-Strand DNA Systems Computed at the B3LYP-D/6−311g(d,p) Level of Theory

system	HOCO (eV)	LUCO (eV)
poly(A)	18.22	9.72
poly(T)	4.08	22.33
poly(G)	15.77	0.54
poly(C)	4.09	39.81
poly(A-T)	40.23	5.14
poly(G-C)	9.59	19.38

shows that the A and G purine-type bands are pushed significantly upward in energy within the double-stranded poly(A-T) and poly(G-C) structures. As mentioned previously, the nucleobases in all four of the ssDNA structures are negatively charged, and the Coulombic repulsion between these nucleobases within the compact dsDNA structure results in an upward shift (i.e., a destabilization) of the A and G bands. As such, the renormalization of the dsDNA band structures causes the highest-filled orbitals to be only localized on the A and G nucleobases, which corroborates the HOCO-localization trends depicted in Figure 6.

Finally, it is worth mentioning that our calculations predict poly(A-T) to be an electron conductor, whereas poly(G-C) is a better hole conductor. The electronic charge per nucleobase in the dsDNA structures also corroborates these trends in electron/hole mobilities. Table 3 shows that poly(A), poly(T), poly(G), and poly(C) have charges of −0.26*e*, −0.20*e*, −0.24*e*, and −0.18*e* per nucleobase, respectively. These electronic charges are correlated with trends where nucleobases with the most negative charge have the highest electron mobilities, whereas nucleobases with the least negative charge have higher hole mobilities. Moving to the dsDNA structures, Table 3 shows that the total charge per A-T and G-C Watson−Crick pair in the poly(A-T) and poly(G-C) structures is −0.47*e* and −0.38*e*, respectively, which reflects the trends in electron/hole mobilities discussed previously. It is interesting to point out that we also observed similar electron/hole mobility trends with LDA since this functional also predicts accurate dsDNA geometries (even though LDA predicts severely underestimated band gaps compared to B3LYP-D). In contrast, the BLYP and B3LYP results give spurious results for electron/hole mobilities (cf. Tables S1 and S2) since these functionals produced deformed dsDNA geometries (cf. Figure 3). As such, these results emphasize the importance of including dispersion effects when calculating electronic properties on self-consistent optimized geometries (using the same functional) for these systems.

CONCLUSIONS

In conclusion, we have carried out large-scale DFT calculations to systematically analyze the structural and electron/hole transport properties of fully periodic single- and double-stranded DNA. To understand how these periodic nucleobase structures are affected by their optimized geometry and underlying electronic structure, we examined the performance of various exchange−correlation functionals, ranging from local (LDA), semilocal (BLYP), hybrid (B3LYP), and dispersion-corrected hybrid (B3LYP-D) methods. Most notably, the latter calculations are among the first studies of periodic DNA and nucleobase structures using dispersion-corrected hybrid functionals for both full geometry optimizations and electronic band structures.

https://doi.org/10.1021/acs.jpcb.2c09141
J. Phys. Chem. B 2023, 127, 5755−5763

With these optimized geometries and band structures, we used the deformation potential formalism to calculate electron/hole mobilities for all of the various ssDNA and dsDNA structures. Our analysis showed that poly(T) and poly(C) are hole conductors, whereas poly(A) and poly(G) structures are better electron conductors. For the dsDNA structures, we found that the poly(A-T) and poly(G-C) band structures are more than just the "sum of their parts." Specifically, Coulombic repulsion between the nucleobases results in a significant renormalization of the band structure, which causes the highest-filled orbitals (and, hence, hole transport) to be only localized on the A and G nucleobases. These findings are consistent with previous experimental results showing that the HOMO localizes on the purine bases.[59−61] Further analyses of the B3LYP-D orbitals and electronic charges in the dsDNA structures show that poly(A-T) is an electron conductor, whereas poly(G-C) is a better hole conductor. Our calculations also highlight the importance of including dispersion effects when calculating electronic properties for these systems since functionals without dispersion will produce deformed dsDNA geometries with spurious electron/hole mobilities.

Finally, while our work focused on optimized structures and electron/hole mobilities of single- and double-stranded DNA, we anticipate that our calculations could also be applied to other DNA-based materials and applications. In particular, the self-consistent geometries, band structures, and electron/hole mobilities from our B3LYP-D calculations could serve as new reference benchmarks to parameterize other coarse-grained DNA models or QM/MM studies,[62] which require accurate electronic properties as input parameters to enable larger-scale simulations. Additional computational work along these lines, which incorporate thermal fluctuations, would be an insightful avenue for future research since they would more accurately capture DNA dynamics under experimental conditions.[63]

■ ASSOCIATED CONTENT

Supporting Information

The Supporting Information is available free of charge at https://pubs.acs.org/doi/10.1021/acs.jpcb.2c09141.

3D animations of HOCOs and LUCOs for poly(A-T); lattice parameters; band gaps; elastic constants; deformation potential constants; electron/hole effective masses, electron/hole mobilities, and electronic band structures for all ssDNA and dsDNA structures obtained with various exchange−correlation functionals; and Cartesian coordinates of all ssDNA and dsDNA structures optimized at the B3LYP-D/6−31g(d) level of theory (PDF)

Hoco_movie (Mpg)

Luco_movie (Mpg)

■ AUTHOR INFORMATION

Corresponding Author

Bryan M. Wong − *Materials Science & Engineering Program, University of California-Riverside, Riverside, California 92521, United States; Department of Chemistry and Department of Physics & Astronomy, University of California-Riverside, Riverside, California 92521, United States;* orcid.org/0000-0002-3477-8043; Email: bryan.wong@ucr.edu; http://www.bmwong-group.com

Authors

Hyuna Kwon − *Materials Science Division, Lawrence Livermore National Laboratory, Livermore, California 94550, United States;* orcid.org/0000-0002-4828-8598

Anshuman Kumar − *Materials Science & Engineering Program, University of California-Riverside, Riverside, California 92521, United States*

Mauro Del Ben − *Applied Mathematics & Computational Research Division, Lawrence Berkeley National Laboratory, Berkeley, California 94720, United States*

Complete contact information is available at: https://pubs.acs.org/10.1021/acs.jpcb.2c09141

Notes

The authors declare no competing financial interest.

■ ACKNOWLEDGMENTS

This work was supported by the U.S. Department of Energy, Office of Science, Office of Advanced Scientific Computing Research, Scientific Discovery through Advanced Computing (SciDAC) program under Award Number DE-SC0022209. This work used the Advanced Cyberinfrastructure Coordination Ecosystem: Services & Support (ACCESS) Expanse computing cluster at the University of California, San Diego, through allocation TG-ENG160024.

■ REFERENCES

(1) Green, L. N.; Subramanian, H. K. K.; Mardanlou, V.; Kim, J.; Hariadi, R. F.; Franco, E. Autonomous Dynamic Control of DNA Nanostructure Self-Assembly. *Nat. Chem.* **2019**, *11*, 510−520.

(2) Li, Z.; Wang, J.; Li, Y.; Liu, X.; Yuan, Q. Self-Assembled DNA Nanomaterials with Highly Programmed Structures and Functions. *Mater. Chem. Front.* **2018**, *2*, 423−436.

(3) Ke, Y.; Ong, L. L.; Shih, W. M.; Yin, P. Three-Dimensional Structures Self-Assembled from DNA Bricks. *Science* **2012**, *338*, 1177−1183.

(4) Keren, K.; Berman, R. S.; Buchstab, E.; Sivan, U.; Braun, E. DNA-Templated Carbon Nanotube Field-Effect Transistor. *Science* **2003**, *302*, 1380−1382.

(5) Marini, M.; Piantanida, L.; Musetti, R.; Bek, A.; Dong, M.; Besenbacher, F.; Lazzarino, M.; Firrao, G. A Revertible, Autonomous, Self-Assembled DNA-Origami Nanoactuator. *Nano Lett.* **2011**, *11*, 5449−5454.

(6) O'Brien, E.; Holt, M. E.; Thompson, M. K.; Salay, L. E.; Ehlinger, A. C.; Chazin, W. J.; Barton, J. K. The [4Fe4S] Cluster of Human DNA Primase Functions as a Redox Switch Using DNA Charge Transport. *Science* **2017**, *355*, No. eaag1789.

(7) Genereux, J. C.; Barton, J. K. Mechanisms for DNA Charge Transport. *Chem. Rev.* **2010**, *110*, 1642−1662.

(8) Genereux, J. C.; Boal, A. K.; Barton, J. K. DNA-Mediated Charge Transport in Redox Sensing and Signaling. *J. Am. Chem. Soc.* **2010**, *132*, 891−905.

(9) Dai, X.; Li, Q.; Aldalbahi, A.; Wang, L.; Fan, C.; Liu, X. DNA-Based Fabrication for Nanoelectronics. *Nano Lett.* **2020**, *20*, 5604−5615.

(10) Taniguchi, M.; Kawai, T. DNA Electronics. *Phys. E* **2006**, *33*, 1−12.

(11) Tapio, K.; Leppiniemi, J.; Shen, B.; Hytönen, V. P.; Fritzsche, W.; Toppari, J. J. Toward Single Electron Nanoelectronics Using Self-Assembled DNA Structure. *Nano Lett.* **2016**, *16*, 6780−6786.

(12) Vittala, S. K.; Han, D. DNA-Guided Assemblies toward Nanoelectronic Applications. *ACS Appl. Bio Mater.* **2020**, *3*, 2702−2722.

(13) Church, G. M.; Gao, Y.; Kosuri, S. Next-Generation Digital Information Storage in DNA. *Science* **2012**, *337*, 1628.

(14) Goldman, N.; Bertone, P.; Chen, S.; Dessimoz, C.; LeProust, E. M.; Sipos, B.; Birney, E. Towards Practical, High-Capacity, Low-Maintenance Information Storage in Synthesized DNA. *Nature* **2013**, *494*, 77−80.
(15) Lin, K. N.; Volkel, K.; Tuck, J. M.; Keung, A. J. Dynamic and Scalable DNA-Based Information Storage. *Nat. Commun.* **2020**, *11*, No. 2981.
(16) Murphy, C. J.; Arkin, M. R.; Jenkins, Y.; Ghatlia, N. D.; Bossmann, S. H.; Turro, N. J.; Barton, J. K. Long-Range Photoinduced Electron Transfer through a DNA Helix. *Science* **1993**, *262*, 1025−1029.
(17) Hall, D. B.; Holmlin, R. E.; Barton, J. K. Oxidative DNA Damage through Long-Range Electron Transfer. *Nature* **1996**, *382*, 731−735.
(18) Dandliker, P. J.; Holmlin, R. E.; Barton, J. K. Oxidative Thymine Dimer Repair in the DNA Helix. *Science* **1997**, *275*, 1465−1468.
(19) Núñez, M. E.; Hall, D. B.; Barton, J. K. Long-Range Oxidative Damage to DNA: Effects of Distance and Sequence. *Chem. Biol.* **1999**, *6*, 85−97.
(20) Kelley, S. O.; Barton, J. K. Electron Transfer between Bases in Double Helical DNA. *Science* **1999**, *283*, 375−381.
(21) Holmlin, R. E.; Dandliker, P. J.; Barton, J. K. Charge Transfer through the DNA Base Stack. *Angew. Chem., Int. Ed.* **1997**, *36*, 2714−2730.
(22) Kasumov, A. Y.; Kociak, M.; Guéron, S.; Reulet, B.; Volkov, V. T.; Klinov, D. V.; Bouchiat, H. Proximity-Induced Superconductivity in DNA. *Science* **2001**, *291*, 280−282.
(23) Porath, D.; Bezryadin, A.; de Vries, S.; Dekker, C. Direct Measurement of Electrical Transport through DNA Molecules. *Nature* **2000**, *403*, 635−638.
(24) de Pablo, P. J.; Moreno-Herrero, F.; Colchero, J.; Gómez Herrero, J.; Herrero, P.; Baró, A. M.; Ordejón, P.; Soler, J. M.; Artacho, E. Absence of Dc-Conductivity in λ-DNA. *Phys. Rev. Lett.* **2000**, *85*, 4992−4995.
(25) Gómez-Navarro, C.; Moreno-Herrero, F.; de Pablo, P. J.; Colchero, J.; Gómez-Herrero, J.; Baró, A. M. Contactless Experiments on Individual DNA Molecules Show No Evidence for Molecular Wire Behavior. *Proc. Natl. Acad. Sci. U.S.A.* **2002**, *99*, 8484−8487.
(26) Hawke, L. G. D.; Kalosakas, G.; Simserides, C. Electronic Parameters for Charge Transfer along DNA. *Eur. Phys. J. E* **2010**, *32*, 291−305.
(27) Klotsa, D.; Römer, R. A.; Turner, M. S. Electronic Transport in DNA. *Biophys. J.* **2005**, *89*, 2187−2198.
(28) Tassi, M.; Morphis, A.; Lambropoulos, K.; Simserides, C. RT-TDDFT Study of Hole Oscillations in B-DNA Monomers and Dimers. *Cogent Phys.* **2017**, *4*, No. 1361077.
(29) Deng, A.; Li, H.; Bo, M.; Huang, Z.; Li, L.; Yao, C.; Li, F. Understanding Atomic Bonding and Electronic Distributions of a DNA Molecule Using DFT Calculation and BOLS-BC Model. *Biochem. Biophys. Rep.* **2020**, *24*, No. 100804.
(30) Olofsson, J.; Larsson, S. Electron Hole Transport in DNA. *J. Phys. Chem. B* **2001**, *105*, 10398−10406.
(31) Biswas, P. K.; Chakraborty, S. Targeted DNA Oxidation and Trajectory of Radical DNA Using DFT Based QM/MM Dynamics. *Nucleic Acids Res.* **2019**, *47*, 2757−2765.
(32) Woźniak, A. P.; Leś, A.; Adamowicz, L. Theoretical Modeling of DNA Electron Hole Transport through Polypyrimidine Sequences: A QM/MM Study. *J. Mol. Model.* **2019**, *25*, No. 97.
(33) Landi, A.; Capobianco, A.; Peluso, A. The Time Scale of Electronic Resonance in Oxidized DNA as Modulated by Solvent Response: An MD/QM-MM Study. *Molecules* **2021**, *26*, No. 5497.
(34) Wang, H.; Lewis, J. P.; Sankey, O. F. Band-Gap Tunneling States in DNA. *Phys. Rev. Lett.* **2004**, *93*, No. 016401.
(35) Gervasio, F. L.; Carloni, P.; Parrinello, M. Electronic Structure of Wet DNA. *Phys. Rev. Lett.* **2002**, *89*, No. 108102.
(36) Artacho, E.; Machado, M.; Sánchez-Portal, D.; Ordejón, P.; Soler, J. M. Electrons in Dry DNA from Density Functional Calculations. *Mol. Phys.* **2003**, *101*, 1587−1594.
(37) Taniguchi, M.; Kawai, T. Electronic Structures of *A*- and *B*-Type DNA Crystals. *Phys. Rev. E* **2004**, *70*, No. 011913.
(38) Bende, A.; Bogár, F.; Ladik, J. Model Calculations of the Energy Band Structures of Double Stranded DNA in the Presence of Water and Na^+ Ions. *Solid State Commun.* **2011**, *151*, 301−305.
(39) Bende, A.; Bogár, F.; Ladik, J. Hole Mobilities of Periodic Models of DNA Double Helices in the Nucleosomes at Different Temperatures. *Chem. Phys. Lett.* **2013**, *565*, 128−131.
(40) Dovesi, R.; Orlando, R.; Erba, A.; Zicovich-Wilson, C. M.; Civalleri, B.; Casassa, S.; Maschio, L.; Ferrabone, M.; De La Pierre, M.; D'Arco, P.; et al. CRYSTAL14: A Program for the Ab Initio Investigation of Crystalline Solids. *Int. J. Quantum Chem.* **2014**, *114*, 1287−1317.
(41) Foster, M. E.; Wong, B. M. Nonempirically Tuned Range-Separated DFT Accurately Predicts Both Fundamental and Excitation Gaps in DNA and RNA Nucleobases. *J. Chem. Theory Comput.* **2012**, *8*, 2682−2687.
(42) Raeber, A. E.; Wong, B. M. The Importance of Short-and Long-Range Exchange on Various Excited State Properties of DNA Monomers, Stacked Complexes, and Watson−Crick Pairs. *J. Chem. Theory Comput.* **2015**, *11*, 2199−2209.
(43) Hohenberg, P.; Kohn, W. Inhomogeneous Electron Gas. *Phys. Rev.* **1964**, *136*, B864−B871.
(44) Becke, A. D. Density-Functional Exchange-Energy Approximation with Correct Asymptotic Behavior. *Phys. Rev. A* **1988**, *38*, 3098−3100.
(45) Becke, A. D. Density-functional Thermochemistry. III. The Role of Exact Exchange. *J. Chem. Phys.* **1993**, *98*, 5648−5652.
(46) Grimme, S. Accurate Description of van Der Waals Complexes by Density Functional Theory Including Empirical Corrections. *J. Comput. Chem.* **2004**, *25*, 1463−1473.
(47) Bardeen, J.; Shockley, W. Deformation Potentials and Mobilities in Non-Polar Crystals. *Phys. Rev.* **1950**, *80*, 72−80.
(48) Shuai, Z.; Wang, L.; Song, C. Deformation Potential Theory. In *Theory of Charge Transport in Carbon Electronic Materials*; Shuai, Z.; Wang, L.; Song, C., Eds.; Springer Berlin: Heidelberg, 2012; pp 67−88.
(49) Jurečka, P.; Šponer, J.; Černý, J.; Hobza, P. Benchmark Database of Accurate (MP2 and CCSD(T) Complete Basis Set Limit) Interaction Energies of Small Model Complexes, DNA Base Pairs, and Amino Acid Pairs. *Phys. Chem. Chem. Phys.* **2006**, *8*, 1985−1993.
(50) Burns, L. A.; Mayagoitia, A. V.; Sumpter, B. G.; Sherrill, C. D. Density-Functional Approaches to Noncovalent Interactions: A Comparison of Dispersion Corrections (DFT-D), Exchange-Hole Dipole Moment (XDM) Theory, and Specialized Functionals. *J. Chem. Phys.* **2011**, *134*, No. 084107.
(51) Wong, B. M.; Hsieh, T. H. Optoelectronic and Excitonic Properties of Oligoacenes: Substantial Improvements from Range-Separated Time-Dependent Density Functional Theory. *J. Chem. Theory Comput.* **2010**, *6*, 3704−3712.
(52) Wong, B. M.; Piacenza, M.; Sala, F. D. Absorption and Fluorescence Properties of Oligothiophene Biomarkers from Long-Range-Corrected Time-Dependent Density Functional Theory. *Phys. Chem. Chem. Phys.* **2009**, *11*, 4498.
(53) Wong, B. M.; Cordaro, J. G. Coumarin Dyes for Dye-Sensitized Solar Cells: A Long-Range-Corrected Density Functional Study. *J. Chem. Phys.* **2008**, *129*, No. 214703.
(54) Wong, B. M.; Ye, S. H. Self-Assembled Cyclic Oligothiophene Nanotubes: Electronic Properties from a Dispersion-Corrected Hybrid Functional. *Phys. Rev. B* **2011**, *84*, No. 075115.
(55) Wong, B. M.; Cordaro, J. G. Electronic Properties of Vinylene-Linked Heterocyclic Conducting Polymers: Predictive Design and Rational Guidance from DFT Calculations. *J. Phys. Chem. C* **2011**, *115*, 18333−18341.
(56) Allec, S. I.; Wong, B. M. Inconsistencies in the Electronic Properties of Phosphorene Nanotubes: New Insights from Large-Scale DFT Calculations. *J. Phys. Chem. Lett.* **2016**, *7*, 4340−4345.
(57) Zhang, I. Y.; Wu, J.; Xu, X. Extending the Reliability and Applicability of B3LYP. *Chem. Commun.* **2010**, *46*, 3057−3070.
(58) Černý, J.; Kabeláč, M.; Hobza, P. Double-Helical → Ladder Structural Transition in the B-DNA Is Induced by a Loss of Dispersion Energy. *J. Am. Chem. Soc.* **2008**, *130*, 16055−16059.

https://doi.org/10.1021/acs.jpcb.2c09141
J. Phys. Chem. B 2023, 127, 5755−5763

(59) Steenken, S.; Jovanovic, S. V. How easily oxidizable is DNA? One-electron reduction potentials of adenosine and guanosine radicals in aqueous solution. *J. Am. Chem. Soc.* **1997**, *119*, 617−618.
(60) Venkatramani, R.; Keinan, S.; Balaeff, A.; Beratan, D. N. Electronic Coupling between Metal Centers and Proteins: Implications for Electron Transfer and the Design of New Materials. *Coord. Chem. Rev.* **2011**, *255*, 635−648.
(61) Kawai, K.; Hayashi, M.; Majima, T. HOMO Energy Gap Dependence of Hole-Transfer Kinetics in DNA. *J. Am. Chem. Soc.* **2012**, *134*, 4806−4811.
(62) Chen, W.; Sun, L.; Tang, Z.; Ali, Z. A.; Wong, B. M.; Chang, C.-E. A. An MM and QM Study of Biomimetic Catalysis of Diels-Alder Reactions Using Cyclodextrins. *Catalysts* **2018**, *8*, No. 51.
(63) Grozema, F. C.; Berlin, Y. A.; Siebbeles, L. D. A. Hole Mobility in DNA: Effects of Static and Dynamic Structural Fluctuations. *ChemPhysChem* **2002**, *3*, 536−539.

https://doi.org/10.1021/acs.jpcb.2c09141
J. Phys. Chem. B 2023, 127, 5755−5763